A Correlation of High Subsonic Afterbody Drag in the Presence of a Propulsive Jet or Support Sting

H. McDonald* and P. F. Hughes†
British Aircraft Corp., Preston, Lancashire, England

The problem of predicting the afterbody contribution to the fuselage form drag at subsonic speeds in the presence of a propulsive jet, support sting, or blunt base is treated by a correlation method. The method includes both curved and conical bodies of revolution below the drag rise Mach number, provided separation of the boundary layer over the body is avoided. In the jet-flow case, at present, the method is restricted to convergent propulsive nozzles but the effect of jet-pressure ratio and temperature is accounted for. From the results it can be seen that afterbody drag can account for as much as 30% of the subsonic profile drag of a typical fighter-type aircraft.

Nomenclature

C_{D0} = aircraft profile drag coefficient based on wing area
C_{DA} = afterbody drag coefficient based on body maximum cross-sectional area $D/q_\infty[(\pi/4)D_m{}^2]$
C_{Db} = base drag coefficient based on body maximum cross-sectional area
$C_{D\beta}$ = boat-tail drag coefficient based on body maximum cross-sectional area
$C_{D\beta z}$ = zero jet-flow boat-tail drag coefficient
C_{pbz} = zero jet-flow base-pressure coefficient
δC_p = increment in base pressure due to sting angle effect
D_b = base diameter
D_j = jet diameter
D_m = body maximum diameter
D_s = sting diameter
H_j = propulsive jet total pressure
l = length from base to sting angle
M = freestream Mach number
p_b = base pressure
p_∞ = freestream static pressure
q_∞ = freestream dynamic pressure
r = radius of sting
T_j = jet temperature, °F
θ = sting conical frustum angle
ζ = $(1 + M^2)^{1/2}$
β = boat-tail angle
ΔC_p = base-pressure increment
L = length of sting conical frustum

1.0 Introduction

THE operation of modern high-speed aircraft over a range of subsonic and supersonic speeds with widely varying engine conditions inevitably involves flying with large base areas at subsonic cruise conditions. It has been realized for some time now that the presence of base area can give rise to an extremely large drag, usually referred to as "afterbody drag." Naturally this drag has been of considerable interest, and the present correlation represents an attempt to provide a rapid means of estimating it.

A related problem to the foregoing arises in the case of support sting interference. Here the practice of mounting a wind tunnel model by means of a support sting (usually designed to simulate the propulsive jet geometry) can lead to unrepresentative air flow over the afterbody. This unrepresentative airflow is, of course, highly undesirable, and an aim of the present work has been to provide a guide to enable the flow to be made as representative as possible.

First of all, the origin of afterbody drag is discussed, and this is followed by a correlation of data on axisymmetric blunt-based bodies. The analysis is then extended to cover the influence of the propulsive jet or support sting.

Received July 30, 1964; revision received November 13, 1964.
* Senior Engineer, Propulsion Group, Preston Division.
† Engineer, Propulsion Group, Preston Division.

2.0 Origin of Afterbody Drag at Subsonic Speeds

The ideal pressure distribution around a body of revolution is given in Fig. 1. The pressure integral in the axial direction is zero for the ideal potential flow case. In practice, the pressure distribution over the body is, of course, slightly different because of the presence of the boundary layer, and the pressure integral in the axial direction is no longer zero. The resulting force is normally termed the form drag of the body. The sum of the skin-friction and form drag is called the profile drag of the body.

Consider now the case of this body truncated at some station 2. Curve 0–1 shows the actual pressure distribution before truncation, and curve 0–2 shows the pressure distribution after truncation. Evidently full recompression over the rear of the body is not achieved after truncation, and, in fact, both the forebody and afterbody form drag have been increased, resulting in a large increase in over-all body profile drag.

For convenience, afterbody drag is split up into two parts, base drag C_{Db} and boat-tail drag $C_{D\beta}$. Base drag is defined to be the integral of the pressure over the rearward facing area normal to the freestream. This is assumed to exclude that area of the base filled by the propulsive jet. Boat-tail drag is defined as the integral of the surface pressures in a rearward direction over the afterbody but excluding the base. Figure 2 defines some of the geometrical parameters involved.

3.0 Simplification of the Problem

To obtain a solution to the problem it is necessary to neglect the change in skin-friction drag resulting from truncating the body. This represents a reasonable approximation when the skin-friction drag is only a small portion of the afterbody drag. It readily is verified a posteriori that this condition is nearly always fulfilled. This reduces the profile drag problem to a form drag problem.

Further simplification is obtained when it is realized that, with a long slender fuselage, the forebody and afterbody may be treated separately. This statement at first sight might seem odd, referred as it is to subsonic speeds where disturbances can affect the flow both at infinity upstream and downstream. In practical terms, however, even in potential flow, rather large changes in geometry of the forebody or afterbody do not, in fact, alter the pressure distribution over the afterbody or forebody, respectively. Even the forebody boundary layer tends to lose its memory during the flow along the long, cylindrical, center section. As a result of this

further approximation, the problem is reduced from a fuselage form drag problem to an afterbody form drag problem.

It follows from the foregoing that, under the terms of the approximation, the fuselage profile drag is slightly overestimated by the sum of the afterbody form drag and the untruncated body profile drag and slightly underestimated by the sum of the afterbody form drag and the forebody profile drag.

4.0 Method of Correlation

The crux of the present correlation lies in the fact that, for a given geometry, there appears to be a unique relationship between the base pressure and the boat-tail drag, independent of the mode of obtaining the base pressure. Furthermore, this relationship seems to be essentially linear over the greater part of the base-pressure range. These points are illustrated in Fig. 3 where the similarity in boat-tail drag at a given base pressure with sting and jet flow is evident. Correlation of one point on this curve, say the zero jet-flow case, together with the gradient of this linear relationship, against the geometric variables, provides a very convenient starting point. In view of the difficulty of obtaining exactly similar geometries to compare sting and jet effects for Fig. 3, sting effect was correlated first of all and interpolated for at the geometry where jet-flow results were obtainable. It follows from this that, in order to estimate the afterbody drag in some condition, it is only necessary to estimate the change in base pressure relative to the chosen reference condition of zero jet flow. The remainder of the correlation is, therefore, concerned with providing a reasonable estimate of this base-pressure change.

5.0 Details of the Correlation

In the subsequent work, experimental data have been analyzed.[1–24]

5.1 Zero Jet Flow

In Fig. 4 the zero flow boat-tail drag $C_{D\beta_z}$ is plotted against the base-to-maximum body diameter ratio D_b/D_m for various boat-tail angles β. From this, knowing the ratio of base-to-maximum body diameter and the boat-tail angle, the zero flow boat-tail drag of circular arc, parabolic, or conical bodies of revolution may be determined by direct interpolation. Obviously, various crossplots of this figure can be made and would prove very useful in practice. In the interest of space, this is left to the individual user.

In Fig. 5 the zero flow base pressure C_{pb_z} is plotted against base-to-maximum body diameter for various boat-tail angles on circular arc and parabolic bodies of revolution. In Fig. 6 a similar plot is given for conical bodies, it being noted that the conical data did not agree with either the circular arc or

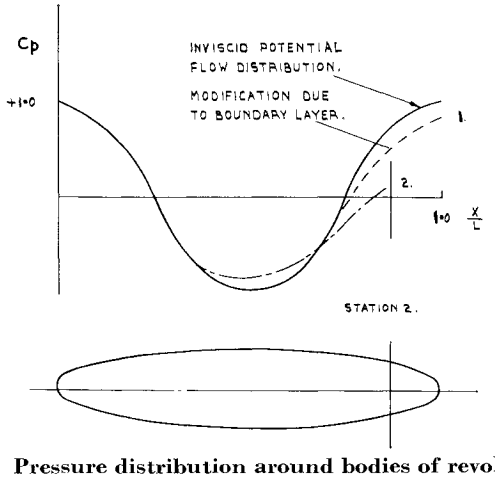

Fig. 1 Pressure distribution around bodies of revolution.

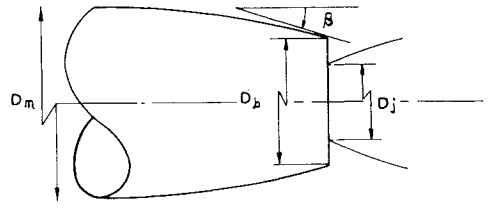

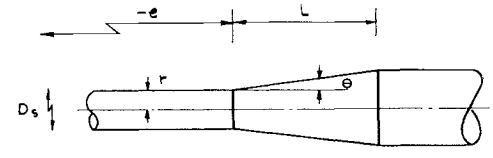

Fig. 2 Sketch of afterbody and sting.

the parabolic data. It was found that, for the conical bodies, boat-tail angles above 8° were liable to result in large, transonic drag rise effects and so were excluded from this investigation.

By use of plots similar to Fig. 3, the rate of change of boat-tail drag with base pressure $\partial C_{D\beta}/\partial C_{pb}$ was determined and is plotted against boat-tail angle in Fig. 7. Thus, for a given geometry, one point and the gradient of the line through the point can be determined on the plot of boat-tail drag against base pressure. The correlation is now concerned with estimating the change in base pressure from the reference condition of zero jet flow.

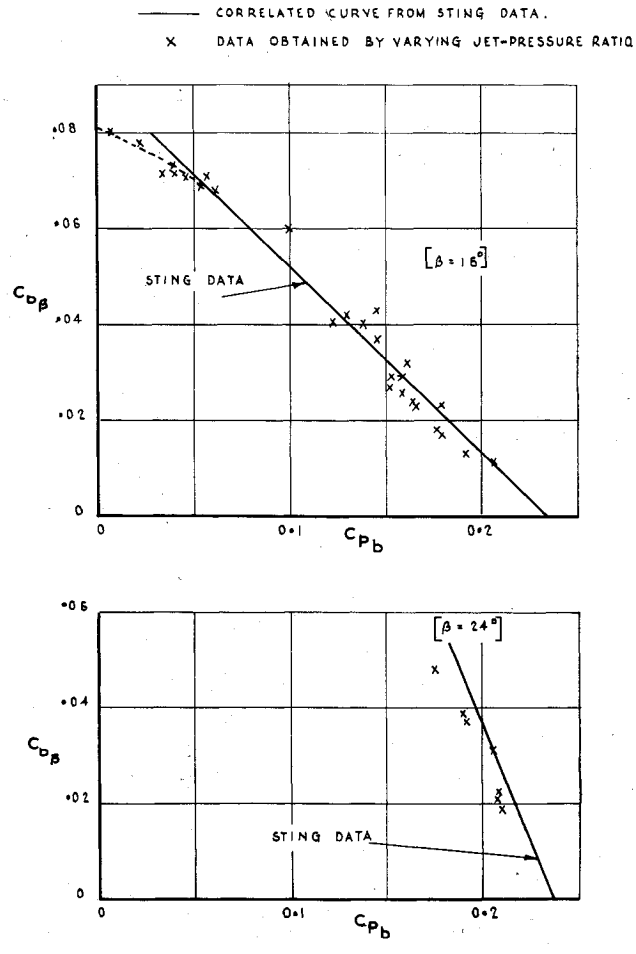

Fig. 3 Boat-tail drag variation with base pressure: a comparison with jet-pressure ratio and sting effect.

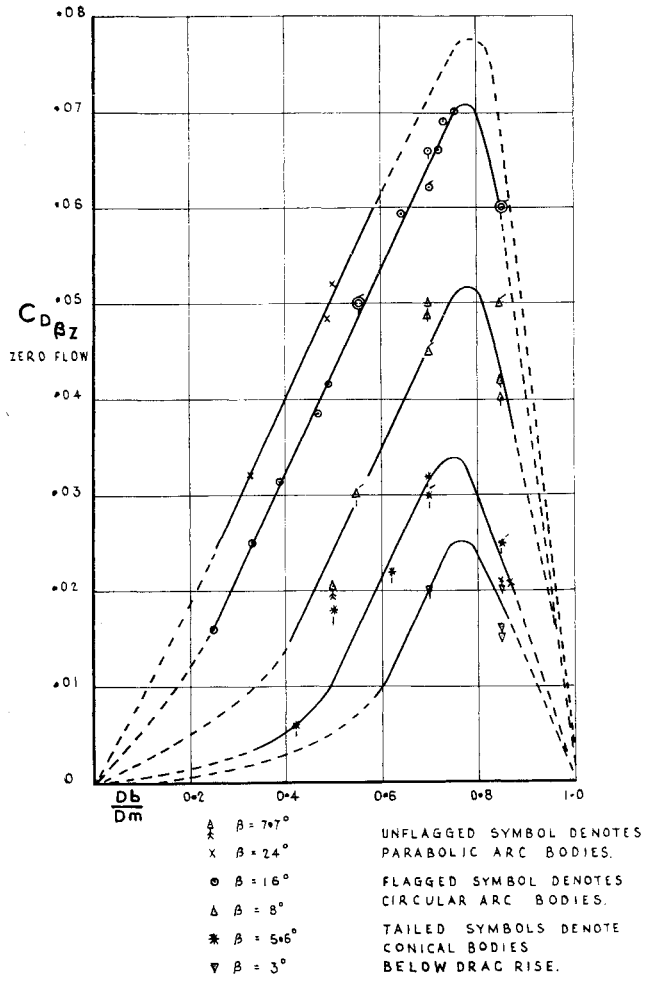

Fig. 4 Zero flow boat-tail drag vs diameter ratio.

5.2 Effect of the Propulsive Jet

It is shown in Fig. 8 that the increment in base pressure due to the propulsive jet plots linearly against a jet to base-to-maximum body diameter function D_j^2/D_bD_m for various jet total pressure ratios and temperatures at boat-tail angles other than zero. These curves are extrapolated to give a hypothetical base-pressure increment ΔC_p at zero jet-diameter ratio D_j (which incidentally was found to be independent of temperature effects). In Fig. 9 this increment is plotted against jet total pressure ratio for various boat-tail angles. In addition, the gradient of the linear relationship $\partial\Delta C_p/\partial(D_j^2/D_bD_m)$ is plotted against jet total-pressure ratio in Fig.

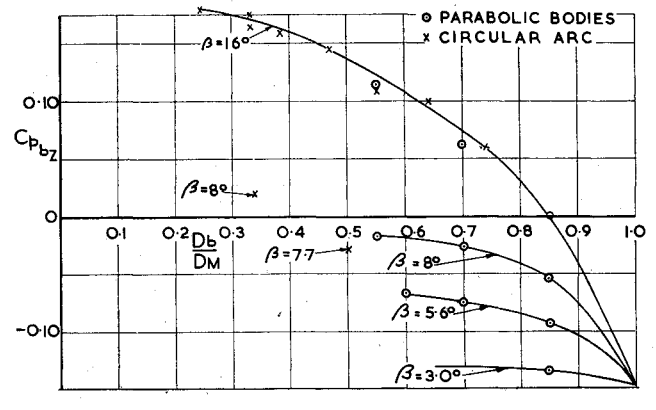

Fig. 5 Zero flow base pressure vs diameter ratio for parabolic and circular arc bodies with various boat-tail angles at $M = 0.9$.

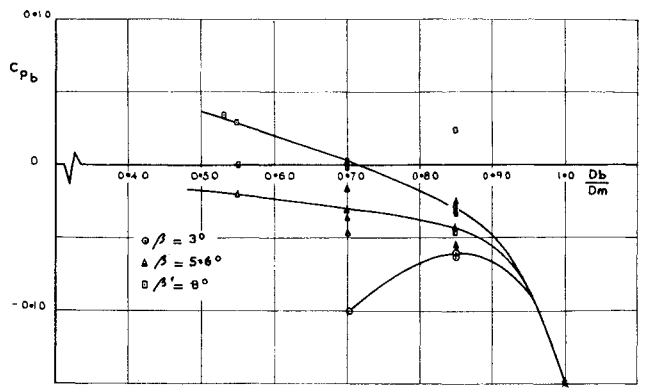

Fig. 6 Zero flow base pressure vs diameter ratio for conical bodies at various boat-tail angles.

10. This gradient was found to be independent of boat-tail angle, but a function of jet temperature. Thus the increment in base pressure due to the propulsive jet can be obtained from a relationship of the form

$$\Delta C_p = \Delta C_p\left(\frac{D_j^2}{D_bD_m} = 0\right) + \frac{\partial\Delta C_p}{\partial(D_j^2/D_bD_m)}\cdot\frac{D_j^2}{D_bD_m} \cdots \quad (1)$$

with the necessary constants obtained from Figs. 9 and 10.

Plotted in Fig. 11 are some data on cylindrical afterbodies, that show the different nature of the problem at zero boat-tail angle. These data have not proved suitable for analysis in the fashion adopted for the other boat-tail angles. If information is required for a cylindrical afterbody, an interpolation should be made directly on Fig. 11.

From the derived value of ΔC_p, the corresponding afterbody drag C_{D_A} based on maximum body cross-sectional area is given as

$$C_{D_A} = C_{D_b} + C_{D_\beta} \quad (2)$$

$$C_{D_b} = -\left(\frac{D_b^2 - D_j^2}{D_m^2}\right)(C_{p_{bz}} + \Delta C_p) \quad (3)$$

$$C_{D_\beta} = C_{D_{\beta z}} + \partial C_{D_\beta}/\partial C_{p_b}\cdot\Delta C_p \quad (4)$$

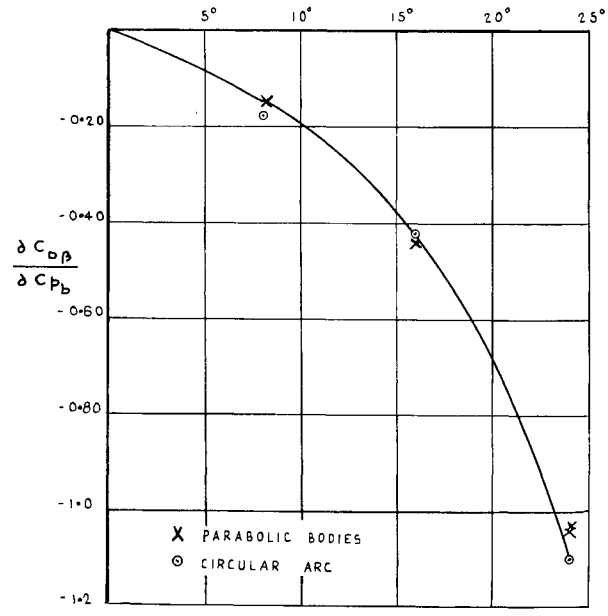

Fig. 7 Rate of change of boat-tail drag with base pressure vs boat-tail angle (available data independent of D_b/D_m).

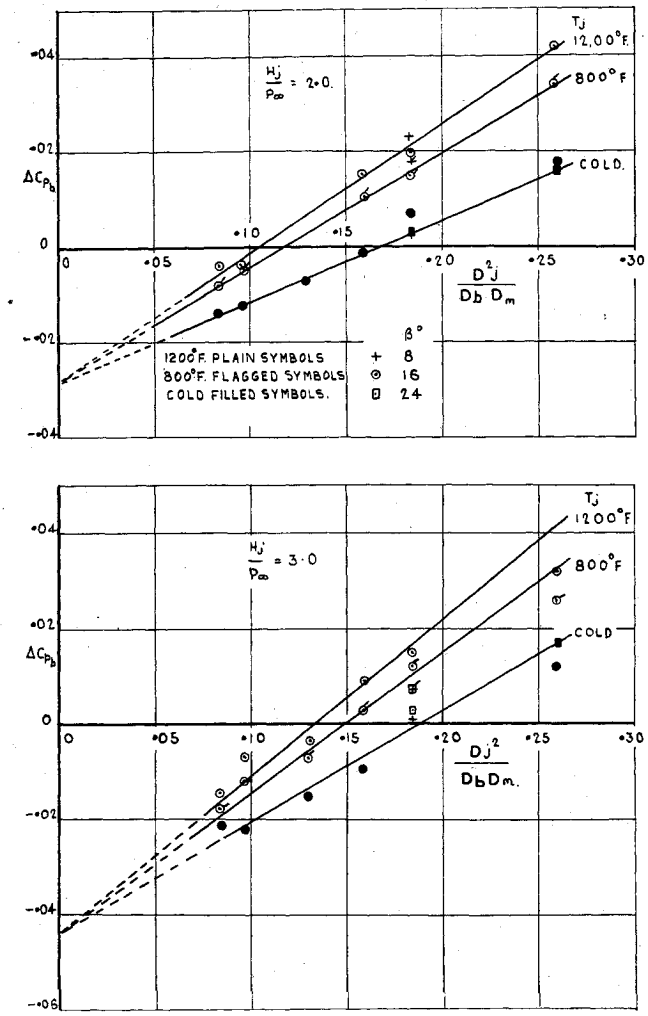

Fig. 8 Base-pressure increment due to jet-pressure ratio and temperature at $M = 0.9$.

5.3 Effect of the Support Sting

Sting effect on base pressure is idealized into two parts, sting-diameter effect and sting-angle effect (see Fig. 2). The sting-diameter effect arises if the sting is considered as a parallel rod stretching downstream to infinity, and the sting diameter varied for a given afterbody geometry. Sting-angle effect arises, however, if the sting is considered as a parallel rod that merges into another parallel rod by means of a conical

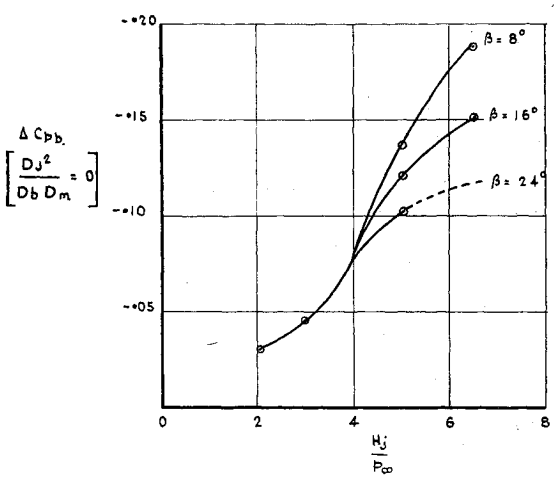

Fig. 9 Extrapolated C_{pb} at zero jet-diameter ratio function (ΔC_{pb} at $D_j^2/D_bD_m = 0$ obtained from plots similar to Fig. 8 and is independent of jet temperature).

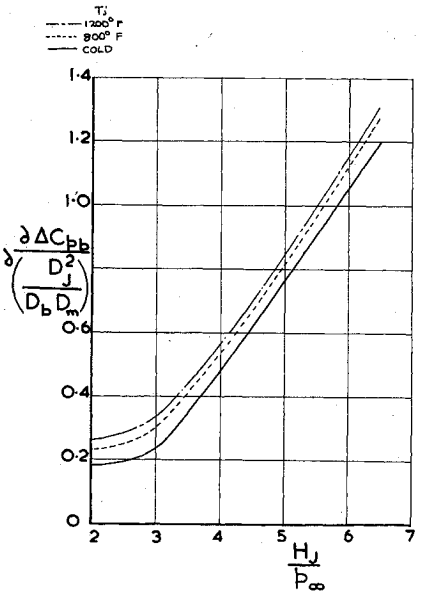

Fig. 10 Gradient of base-pressure increment jet-diameter ratio (gradient of ΔC_{pb} vs D_j^2/D_bD_m obtained from plots similar to Fig. 8 and valid for all boat-tail angles except zero).

frustum and the angle and position of this frustum as varied for a given afterbody geometry and a given sting initial diameter. The two effects are considered separately and assumed additive.

It was found that the sting-diameter effect could be correlated on a basis of sting-to-base area, sensibly independent of the maximum cross section, and a function of boat-tail angle

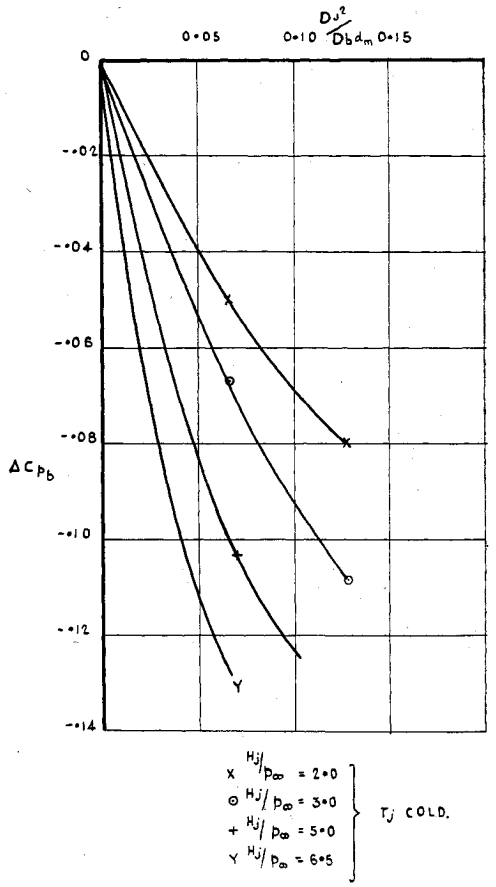

Fig. 11 Base-pressure increment due to jet-pressure ratio at $M = 0.9$ on cylindrical afterbodies.

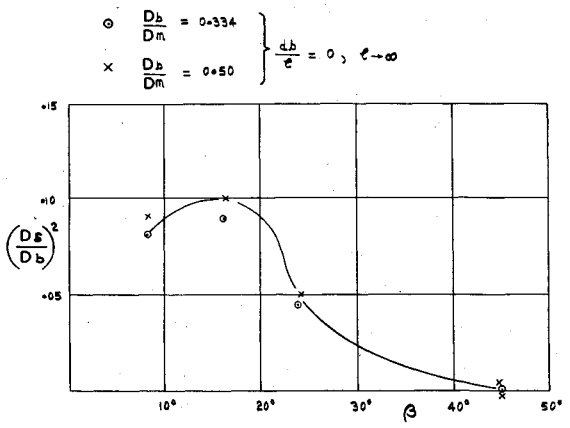

Fig. 12 Sting-diameter effect on base pressure at M = 0.9.

only. This correlation is given in Fig. 12 where the rate of change of base pressure with sting-to-base area is given as a function of boat-tail angle. From this, the base pressure resulting from a parallel sting can be obtained from

$$C_p = C_{pbz} + \frac{\partial C_{pb}}{\partial (D_s/D_b)^2} \cdot \left(\frac{D_s}{D_b}\right)^2 \tag{5}$$

In Ref. 4 a theoretical expression is derived for the effect of the sting angle and is given as

$$\delta C_p = \tan\theta \left[\frac{1}{\{(l/r)^2 \zeta^2\}^{1/2}} - \frac{(L/r)\tan\theta + 1}{\{[(L/r) - (l/r)]^2 + \zeta^2\}^{1/2}} \right] + \tan^2\theta \left[\sinh^{-1}\left\{ \frac{(L/r) - (l/r)}{\zeta} \right\} - \sinh^{-1}\left\{ \frac{-l/r}{\zeta} \right\} \right] \tag{6}$$

where $\zeta = (1 + M^2)^{1/2}$, M is the freestream Mach number, θ is the semivertex angle of the conical frustum, L the cone length, r the radius of the sting, and $-l$ the upstream distance to the base. The validity of (6) depends upon the $\sinh^{-1}$ function being positive. The equation therefore is applicable only when l is negative. Furthermore, for values of l approaching zero, the small perturbation assumption of the theory is violated.

The base pressure obtained with a sting is assumed to be the sum of the effects given by (5) and (6). From a knowledge of this base pressure, the boat-tail drag can be estimated from a relationship identical to (4). Thus, any tunnel drag can be corrected to some flight condition. It is probably apparent from the earlier remarks that the flow over the afterbody will be duplicated if the base pressure in the presence of the sting is identical to the base pressure in the presence of the propulsive jet. In order to do this, it is only necessary to choose some typical condition with the propulsive jet and estimate the base pressure as indicated in Sec. 5.2; then from the approach outlined previously, the sting geometry can be manipulated to give the required base pressure.

6.0 Some Limitations on the Use of the Data

6.1 Mach Number

The entire analysis was carried out at a freestream Mach number of 0.9, but it was noted that, below this Mach number, little or no variation in afterbody drag occurred except in the case of conical afterbodies with boat-tail angles greater than about 8°. As a result, these conical afterbodies were deleted from the investigation, and a general limit on Mach number may be observed as $0.6 < M < 0.9$.

6.2 Model Geometry

The results presented were derived from tests mainly on conical, parabolic, and circular arc bodies of revolution so that they can only be expected to give reasonable agreement for bodies of similar curvature. Limitations on base pressure are difficult to obtain since these limitations have to be linked to the separation of the boundary layer over the afterbody. Not having sufficient information to do this at present, it can really only be said that parabolic and circular arc bodies with boat-tail angles greater than about 16° should be treated with caution, and for conical afterbodies this angle drops to about 8° in view of the Mach number effects.

It should be noted that, based on the present data, the effect of the propulsive jet on cylindrical afterbodies exhibits a marked difference from the effect at a slight boat-tail angle. Based on Fig. 8, a maximum value D_j^2/D_bD_m of about 0.25 should be observed.

6.3 Propulsive Jet

It has been shown in detail by various investigators that the effect of the nozzle can have a considerable effect on the base pressure at supersonic speeds. In addition to this, the practice of bleeding small quantities of air into the base region is known to give rise to large changes in the base pressure. In view of these remarks, the present correlation should be restricted to convergent nozzles with zero bleed mass flow.

6.4 Reynolds Number Effects

In most of the tests utilized in the correlation, very little effect of Reynolds number was noted. The data on this effect are very sparse, and the results are by no means conclusive.

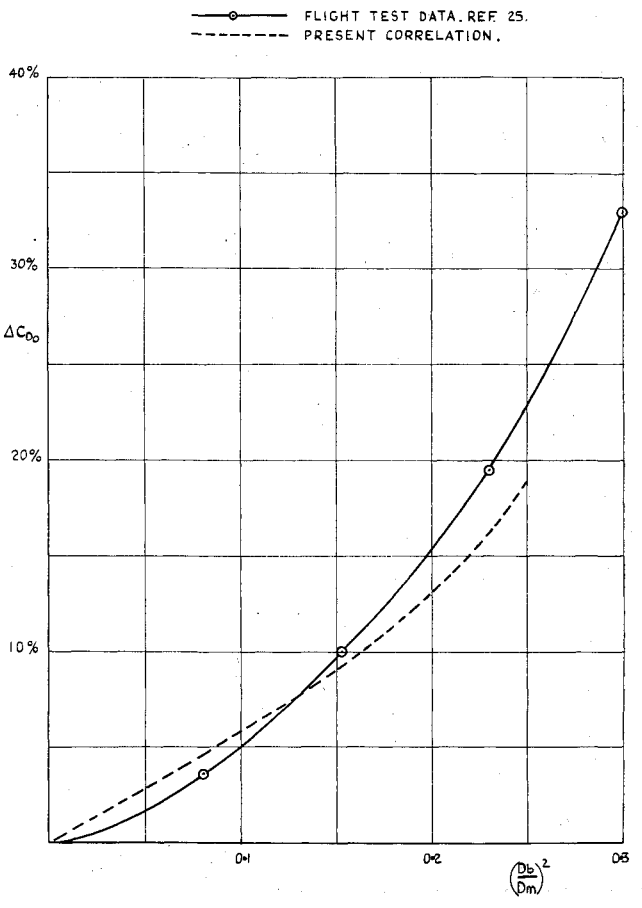

Fig. 13 A comparison between measured and estimated profile-drag increment due to base area (M = 0.7 H_j/P_∞ = 3.0).

It should appear, however, that with the present state of knowledge it is a reasonable assumption to neglect Reynolds number effects.

7.0 Comments and Conclusions

By using the correlation, an estimate was made of the increase in profile drag caused by the base area on an interceptor-type aircraft. This is compared in Fig. 13 with flight test measurements.[25]

It is readily apparent from the comparison that good agreement between predicted and measured afterbody drag has been obtained and that afterbody drag can account for anything between 5 and 30% of a typical fighter-aircraft subsonic profile-drag coefficient and obviously warrants careful consideration. As with most correlations, there is considerable lack of suitable experimental data for inclusion. However, it is felt that sufficient data have been analyzed so that reliable trends can be deduced and the order of magnitude of the drag estimated.

References

[1] Love, E. S., "A summary of information on support interference at transonic and supersonic speeds," NACA RM L53K12 (1953).

[2] Hart, R. C., "Effects of stabilising fins and a rear mounted support sting on the base pressure of a body of revolution in free flight at Mach numbers from 0.1 to 1.3," NACA RM L52E06 (1952).

[3] Cahn, M. S., "An experimental investigation of sting-support effects on drag and a comparison with jet effects at transonic speeds," NACA RM L56F18 (1956).

[4] Tunnell, P. J., "An investigation of sting-support interference on base pressure and forebody chord force at Mach numbers from 0.60 to 1.3," NACA RM A54K16a (1954).

[5] Katz, E. R., "Flight investigation at high subsonic, transonic, and supersonic speeds to determine zero-lift drag of bodies of revolution having fineness ratio of 6.04 and varying positions of maximum diameter," NACA RM L49F02 (1949).

[6] Katz, E. R. and Stoney, W. E., Jr., "Base pressures measured on several parabolic arc bodies of revolution in free flight at Mach numbers from 0.8 to 1.4 and at large Reynolds numbers," NACA RM L51F29 (1951).

[7] Gillespie, W., Jr., "Jet effects on pressures and drag of bodies," NACA RM L51J29 (1951).

[8] Nussdorfer, T., Wilcox, F., and Perchonok, E., "Investigation at zero angle of attack of a 16″ ram jet engine in an 8′ × 6′ supersonic wind tunnel," NACA RM E50L04 (1950).

[9] Fradenburgh, E. A., Gorton, G. C., and Beke, A., "Thrust characteristics of a series of convergent-divergent exhaust nozzles at subsonic and supersonic flight speeds," NACA RM E53L23 (1953).

[10] Salmi, R. J., "Experimental investigation of drag of afterbodies with exiting jet at high subsonic Mach numbers," NACA RM E54I13 (1954).

[11] Falanga, R. A., "Free flight investigation of the effects of simulated sonic turbojet exhaust on the drag of a boat-tail body with various jet sizes from Mach numbers 0.87 to 1.50," NACA RM L55FO9a (1955).

[12] Henry, B. Z., Jr. and Cahn, M. S., "Preliminary results of an investigation at transonic speeds to determine the effects of a heated propulsive jet on the drag characteristics of a related series of afterbodies," NACA L55A24a (1955).

[13] Hoffman, S., "Free flight tests to determine the power on and power off pressure distribution and drag of the NACA RM-10 research vehicle at large Reynolds numbers between Mach numbers 0.8 and 3.0," NACA RM L55HO2 (1955).

[14] Jackson, H. H., Runsey, C. B., and Chauvin, L. T., "Flight measurements of drag and base pressure of a fin stabilised parabolic body of revolution (NACA RM-10) at different Reynolds numbers and at Mach numbers from 0.9 to 3.3, NACA TN 3320 (1954).

[15] Purser, P. E., Thebodaux, J. G., and Jackson, H. H., "Note on some observed effects of rocket-motor operation on the base pressure of bodies in free flight," NACA RM L50I18 (1950).

[16] Peck, R. F., "Flight measurements of base pressure on bodies of revolution with and without simulated rocket chambers," NACA RM L50I28a (1950).

[17] Salini, R. J., "Preliminary investigation of methods to increase base pressure of plug nozzles at Mach 0.9," NACA RM E56J05 (1956).

[18] Henry, B. Z., Jr. and Cahn, M. S., "Additional results of an investigation at transonic speeds to determine the effects of a heated propulsive jet on the drag characteristics of a series of related afterbodies," NACA L56G12 (1956).

[19] Silhan, F. V. and Cubbage, J. M., Jr., "Drag of conical and circular arc, boat-tail afterbodies at Mach numbers from 0.6 to 1.3," NACA RM L56K22 (1956).

[20] Falanga, R. A. and Leiss, A., "Free-flight investigation at transonic speeds of drag coefficients of a boat-tail body of revolution with a simulated turbojet exhaust issuing at the base from conical short length ejectors," NACA RM L56H23 (1956).

[21] Cubbage, J. H., Jr., "Effect of convergent ejector nozzles on the boat-tail drag of a 16° conical afterbody at Mach numbers of 0.6 to 1.26," NACA L58G25 (1958).

[22] Norton, H. T., Jr. and Swihart, J. M., "Effect of a hot jet exhaust on pressure distributions and external drag of several afterbodies on a single-engine airplane model at transonic speeds," NACA RM L57J04 (1957).

[23] Cubbage, J. M., Jr., "Jet effects on the drag of conical afterbodies for Mach numbers of 0.6 to 1.28," NACA RM L57B21 (1957).

[24] Kell, C., "Free-flight measurements of pressure distribution at transonic and supersonic speeds on bodies of revolution having parabolic afterbodies," Royal Aircraft Establishment Rept. Aero. 2605 (1958).

[25] Unpublished flight test data, Bristol Siddeley Engines Ltd., Rept. TED. 23,687; also Gloster Aircraft Technical Dept. of Aeronautics Rept. M83 (March 1960).